Contribution from the Department of Chemistry, University of Missouri-Rolla, Rolla, Missouri 65401, the Nuclear Physics Division, Atomic Energy Research Establishment, Harwell, Didcot, OX11 ORA, England, and the Chemical Crystallography Laboratory, Oxford University, Oxford, OX1 3PD, England

A Study of Anhydrous Iron(III) Sulfate by Magnetic Susceptibility, Mössbauer, and Neutron Diffraction Techniques

GARY J. LONG,*[1a,b] GEOFFREY LONGWORTH,[1b] PETER BATTLE,[1c] ANTHONY K. CHEETHAM,*[1c] RAJU V. THUNDATHIL,[1a] and DAVID BEVERIDGE[1d]

Received July 20, 1978

A powder neutron-diffraction study and subsequent line-profile analysis of the nuclear and magnetic structure at 4.2 K of monoclinic anhydrous iron(III) sulfate indicate that it is a two-sublattice antiferromagnet. Each sublattice is made up of crystallographically distinct iron atoms in the space group $P2_1/n$ (*b*-unique). The nuclear structure at 4.2 K is essentially the same as that found at room temperature by single-crystal X-ray analysis. An analysis of covalency in the material indicates that the degree of covalency is consistent with that found for other iron(III) ions octahedrally coordinated by oxygen. A Mössbauer effect study indicates that above 28.8 K this compound is paramagnetic with parameters typical of an octahedral high-spin iron(III) compound. Below 28.7 K the Mössbauer spectrum reveals the presence of spontaneous magnetic ordering with nonequivalent internal hyperfine fields on the two sublattices. The difference between these fields reaches a maximum at 23 K and decreases until, at 4.2 K, the field on each sublattice is essentially the same at ca. 550 kOe. The two sublattices have essentially the same isomer shifts while the quadrupole shifts are similar in magnitude but opposite in sign. Applied-field Mössbauer effect studies further support an antiferromagnetic coupling model. Magnetic susceptibility studies confirm that the material is paramagnetic with an effective magnetic moment of ca. 5.92 μ_B between 298 and 40 K. Below this temperature the magnetic susceptibility increases sharply to a maximum at 23 K and then decreases rapidly. This behavior results because of the nonequivalent magnitude of the spontaneous magnetization on each sublattice between 28 and 4.2 K. A magnetic superexchange coupling model is proposed to explain the magnetic nonequivalence of the two sublattices over this temperature range.

Introduction

The magnetic properties of many ordered materials have been extensively studied to determine the relation of molecular structure to intermolecular exchange coupling. Many of these properties have been discussed in detail in recent review articles and books.[2-4] It is thus surprising to learn how little is known of the magnetic properties of anhydrous iron(III) sulfate. Essentially, the only data available on the magnetic properties indicate that iron(III) sulfate is ordered[5] at 4.2 K and is paramagnetic in the 289–850 K temperature range.[6] The magnetic-ordering temperature is not known, and, although higher temperature Mössbauer spectra have been reported,[7,8] the low-temperature Mössbauer effect properties have not been studied. Champion et al.[9] have shown that the iron in iron(III) sulfate is reversibly converted to divalent iron at high pressure.

Anhydrous iron(III) sulfate occurs in two crystalline forms, one monoclinic and the other rhombohedral. The room-temperature single-crystal X-ray structure of the monoclinic modification has been determined independently by both Moore and Araki[10] and Christidis and Rentzeperis.[11] The structure consists of an infinite network of iron–oxygen–sulfur linkages in which the oxygen atoms coordinate the iron atoms octahedrally and the sulfur atoms tetrahedrally; the octahedra share corners with the tetrahedra.

We have undertaken a detailed investigation of the magnetic properties of anhydrous iron(III) sulfate. The magnetic susceptibility was studied at the Univerisity of Missouri-Rolla, the Mössbauer spectral properties at AERE, Harwell, and the powder neutron-diffraction data at the Chemical Crystallography Laboratory, Oxford University.

Experimental Section

Anhydrous iron(III) sulfate was prepared by placing 100 g of analytical grade $FeSO_4 \cdot 7H_2O$ and 1 L of concentrated sulfuric acid in a 2-L round-bottom flask. This mixture was refluxed for ca. 4 h. During this time sulfur dioxide was evolved and vented to the atmosphere. The pale pink precipitate which formed was filtered via reduced pressure, washed with sulfuric acid and acetone, and air-dried. The product is air stable and does not take up water from the atmosphere—at least during short periods of the order of several hours. It appears to be stable indefinitely when stored in a desiccator. Iron(III) was determined by titration[12] with mercury(I) nitrate. Anal. Calcd for $Fe_2S_3O_{12}$: Fe, 27.93. Found: Fe, 28.25. The X-ray powder diffraction pattern for this sample was obtained with a Guinier camera. The resulting pattern is in excellent agreement with that expected for the monoclinic form of iron(III) sulfate and exhibited no lines which would be attributed to the rhombohedral form. We estimate that our sample could contain no more than ca. 1% of the rhombohedral modification.

Powder neutron-diffraction data were obtained on the D1A powder diffractometer at the Institute Laue-Langevin, Grenoble, France. The germanium monochromator was set to produce a neutron beam with a wavelength of 1.903 Å, the longest wavelength available on D1A. This wavelength was chosen in order to give the maximum peak separation. The wavelength was determined by calibration with a nickel standard. A 2θ scan of the diffraction pattern was obtained at 4.2 K with the sample mounted in a vanadium can which was placed in a helium cryostat with an aluminum tail section. The geometry of the tail section was such that the aluminum peaks did not appear in the diffraction pattern. The group of ten counters was moved in steps of 0.05°. In this way, the region of 2θ between 15° and 135° was scanned such that the intensity at each 0.05° incremental angle was recorded by at least two counters. The data from the different counters were merged by using Hewat's computer program[13] at the ILL. All further data reduction and refinement was performed on the ICL 1906A computer at Oxford University.

The Mössbauer effect spectra were obtained on a Harwell constant-acceleration spectrometer which utilized a room-temperature rhodium-matrix source and was calibrated with natural α-iron foil. The liquid helium spectra were obtained in cryostats in which the sample was placed directly in the liquid helium. The magnetically perturbed spectra were obtained with a British Oxygen Corp. superconducting magnet and cryostat which produced a transverse magnetic field. The magnetic field was calibrated by measuring the change in the iron foil internal hyperfine field produced by the magnet. Temperatures between 4.2 and 78 K were obtained through the use of a variable-temperature insert placed in the liquid helium cryostat. The temperature was measured by a gold–iron thermocouple and was controlled to ±0.1 K. The Mössbauer spectra were evaluated by using least-squares minimization computer programs and the Harwell IBM 370/168 computer facilities.

The magnetic susceptibility measurements were obtained on a Faraday balance which utilized a Janis Supervaritemp helium cryostat and a Lake Shore Cryotronics temperature controller. Temperatures

* To whom correspondence should be addressed at the University of Missouri-Rolla.

0020-1669/79/1318-0624$01.00/0

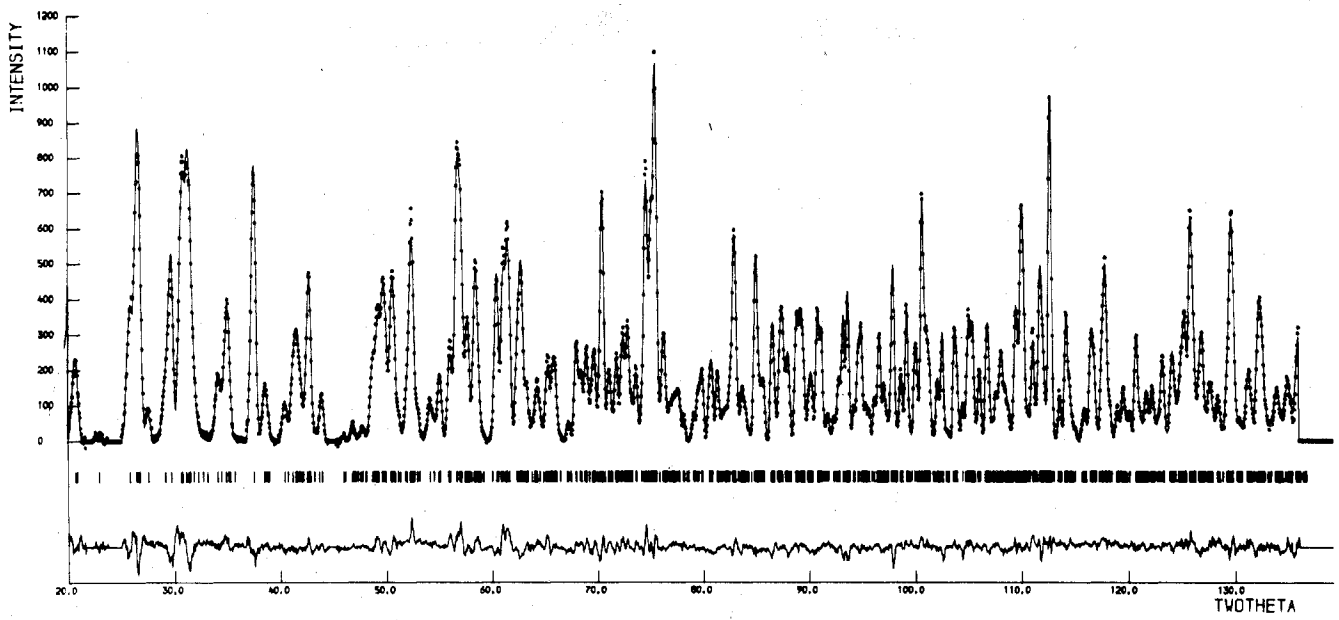

Figure 1. The observed, calculated, and difference profile for the powder neutron-diffraction pattern of $Fe_2(SO_4)_3$ at 4.2 K.

were measured with a calibrated silicon diode and are accurate to ca. 0.1% of the absolute temperature. The magnetic field was measured with a Hall probe gaussmeter and the balance was calibrated[14] with both $CuSO_4 \cdot 5H_2O$ and $CoHg(NCS)_4$. Force measurements were obtained at eight different fields between 1000 and 8000 G.

Results and Discussion

Neutron Diffraction Results. The 4.2 K neutron diffraction pattern was indexed in the space group[10] $P2_1/n$ (*b*-unique) with $a = 11.573$ (3) Å, $b = 8.25$ (3) Å, $c = 8.262$ (3) Å, and $\beta = 90.81$ (1)°. These parameters are in very good agreement with the parameters determined by using X-rays at room temperature.[10,11,15]

The structure was refined by using the Rietveld line-profile analysis technique.[16] The large vertical divergence of the counters on the D1A causes low-angle diffraction peaks to depart from their ideal Gaussian shape. Consequently, we analyzed only the data with $2\theta > 20°$. The 2270 profile points measured were distributed over 785 reflections. The structure determined at room temperature by Moore and Araki[10] was used as a starting model for the nuclear scattering. This required a total of 51 variable atomic coordinates in addition to an overall temperature factor and the usual profile parameters. The following scattering lengths were used: $b_{Fe} = 0.951$, $b_S = 0.285$, $b_O = 0.58$ ($\times 10^{-14}$ m).

The presence of an intense (110) reflection suggested an antiferromagnetic structure because this peak is weak with respect to nuclear scattering, and the magnetic structure factor is small if a ferromagnetic configuration is assumed. A range of models for the spin configuration was tested. The coupling between crystallographically equivalent iron atoms was found to be ferromagnetic. The most satisfactory refinement was obtained with the magnetic moments of the Fe(1) atoms coupled antiparallel to those of Fe(2) and lying in the *ac* plane. With this spin arrangement, the magnetic cell retains the monoclinic symmetry of the atomic cell.

The magnetic and nuclear structures were refined simultaneously. The value of the magnetic moment on Fe(1) was constrained to equal that on Fe(2). A free-ion magnetic form factor was adopted.[18] Refinements with expanded or contracted form factors gave slightly higher *R* values. A study of the iron(III) form factor in yttrium–iron garnet also favors the free-ion curve for the octahedral site.[19] We found no evidence of a "ligand peak" in the form factor.[20] The final value of the magnetic moment was 4.52 (8) μ_B, with components $k_x = 3.88$ (6) μ_B and $k_z = 2.36$ (12) μ_B. The overall temperature factor was 0.02(1) Å^2. Final atomic coordinates are given in Table I[21] and bond lengths and bond angles are shown in Table II. The observed and calculated diffraction patterns are illustrated in Figure 1. The resulting structure is presented in Figure 2.

Table I. Final Atomic Positional Parameters for Anhydrous Iron(III) Sulfate at 4.2 K

atom	*x*	*y*	*z*
Fe(1)	0.1151 (3)	0.0356 (3)	0.2473 (3)
Fe(2)	0.3834 (3)	0.0335 (3)	0.7515 (3)
S(1)	0.5042 (9)	0.2490 (10)	0.4623 (9)
S(2)	0.1493 (8)	0.3822 (8)	0.3942 (9)
S(3)	0.3549 (8)	0.3861 (9)	0.8910 (8)
O(1)	0.6029 (4)	0.3099 (4)	0.5599 (4)
O(2)	0.5522 (4)	0.1717 (4)	0.3166 (4)
O(3)	0.4270 (4)	0.3736 (4)	0.4121 (5)
O(4)	0.4365 (4)	0.1354 (4)	0.5546 (4)
O(5)	0.1787 (4)	0.2139 (5)	0.3731 (4)
O(6)	0.0293 (4)	0.4115 (4)	0.3672 (4)
O(7)	0.1818 (4)	0.4188 (4)	0.5632 (5)
O(8)	0.2205 (4)	0.4763 (4)	0.2878 (4)
O(9)	0.3126 (4)	0.2266 (5)	0.8462 (4)
O(10)	0.3905 (4)	0.3879 (5)	0.0611 (5)
O(11)	0.4511 (4)	0.4256 (4)	0.7862 (5)
O(12)	0.2610 (4)	0.4978 (4)	0.8697 (4)

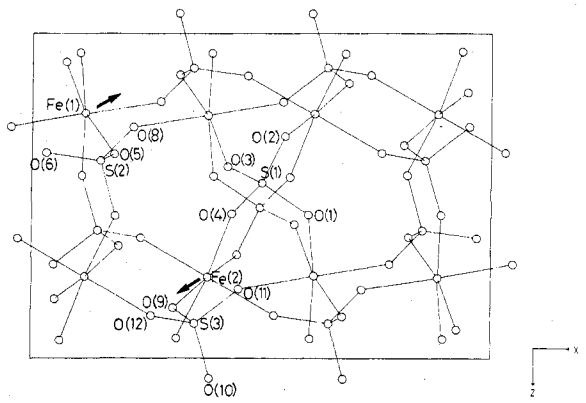

Figure 2. A projection of the atomic and magnetic structure of $Fe_2(SO_4)_3$ at 4.2 K normal to the crystallographic *ac* plane. The unit cell origin is the upper left-hand corner.

Table II. Intramolecular Bond Distances (Å) and Bond Angles (deg) at 4.2 K[a]

Distances			
Fe(1)-O(1)''	2.05 (6)	S(1)-O(1)	1.48 (1)
Fe(1)-O(3)'	1.965 (6)	S(1)-O(2)	1.49 (1)
Fe(1)-O(5)	1.977 (6)	S(1)-O(3)	1.44 (1)
Fe(1)-O(8)'	1.994 (6)	S(1)-O(4)	1.47 (1)
Fe(1)-O(10)'	2.025 (6)	average	1.47
Fe(1)-O(11)''	1.958 (6)	S(2)-O(5)	1.49 (1)
average	1.992	S(2)-O(6)	1.43 (1)
Fe(2)-O(2)'''	1.986 (6)	S(2)-O(7)	1.47 (1)
Fe(2)-O(4)	1.950 (6)	S(2)-O(8)	1.45 (1)
Fe(2)-O(6)''	1.984 (6)	average	1.46
Fe(2)-O(7)'	1.975 (6)	S(3)-O(9)	1.49 (1)
Fe(2)-O(9)	2.002 (6)	S(3)-O(10)	1.46 (1)
Fe(2)-O(12)'	1.960 (6)	S(3)-O(11)	1.46 (1)
average	1.976	S(3)-O(12)	1.45 (1)
		average	1.47

Angles[b]			
O(1)''-Fe(1)-O(3)'	86.0	O(2)'''-Fe(2)-O(4)	91.8
O(1)''-Fe(1)-O(5)	85.1	O(2)'''-Fe(2)-O(6)''	91.4
O(1)''-Fe(1)-O(8)'	96.3	O(2)'''-Fe(2)-O(7)'	86.1
O(1)''-Fe(1)-O(11)''	87.6	O(2)'''-Fe(2)-O(12)'	92.2
O(3)'-Fe(1)-O(8)'	87.2	O(4)-Fe(2)-O(6)''	91.2
O(3)'-Fe(1)-O(10)'	94.4	O(4)-Fe(2)-O(9)	95.5
O(3)'-Fe(1)-O(11)''	89.8	O(4)-Fe(2)-O(12)'	85.4
O(5)-Fe(1)-O(8)'	85.5	O(6)''-Fe(2)-O(7)'	94.3
O(5)-Fe(1)-O(10)'	94.7	O(6)''-Fe(2)-O(9)	88.2
O(5)-Fe(1)-O(11)''	98.0	O(7)'-Fe(2)-O(9)	86.6
O(8)'-Fe(1)-O(10)'	89.9	O(7)'-Fe(2)-O(12)'	89.2
O(10)'-Fe(1)-O(11)''	86.2	O(9)-Fe(2)-O(12)'	88.6
average	90.1	average	90.0
O(1)-S(1)-O(2)	107.6	O(5)-S(2)-O(6)	112.0
O(1)-S(1)-O(3)	111.6	O(5)-S(2)-O(7)	105.0
O(1)-S(1)-O(4)	111.2	O(5)-S(2)-O(8)	109.2
O(2)-S(1)-O(3)	109.3	O(6)-S(2)-O(7)	110.3
O(2)-S(1)-O(4)	109.8	O(6)-S(2)-O(8)	111.6
O(3)-S(1)-O(4)	107.6	O(7)-S(2)-O(8)	108.5
average	109.5	average	109.4
O(9)-S(3)-O(10)	109.7		
O(9)-S(3)-O(11)	108.3		
O(9)-S(3)-O(12)	109.0		
O(10)-S(3)-O(11)	111.2		
O(10)-S(3)-O(12)	108.1		
O(11)-S(3)-O(12)	110.6		
average	109.5		

[a] The primed atoms represent the following transformations: prime, $^1/_2 - x$, $^1/_2 + y$, $^1/_2 - z$; double prime, $^1/_2 + x$, $^1/_2 - y$, $^1/_2 + z$; triple prime, $-x$, $-y$, $-z$. [b] Estimated standard deviation in the bond angles is 1°.

The final reliability factor R_{pr} was 6.7% as calculated from the expression

$$R_{pr} = \left[\frac{\sum_i (w_i y_i(\text{obsd}) - c^{-1} y_i(\text{calcd}))^2}{\sum_i (w_i y_i(\text{obsd}))^2} \right]$$

where y_i(obsd) and y_i(calcd) are the observed and calculated intensities at the ith point on the profile, w_i is the weight applied to the ith observation, and c is the scale factor.

In order to achieve this quality of refinement, it was necessary to apply a correction for preferred orientation. The need for this was shown by the poor agreement between the observed and calculated profiles around several (0kl) reflections, in particular (020), (021), (012), and (022). A subsequent neutron study of the paramagnetic phase of anhydrous iron(III) sulfate[22] has shown that this effect is also present above the Néel temperature; it is not therefore due to an inadequacy in our model for the magnetic structure. The need for a preferred orientation correction is consistent with reports in the literature[8,11] that anhydrous iron(III) sulfate forms platelike crystals, with a the normal to the plate.

Table III. Mössbauer Effect Parameters for Monoclinic, Anhydrous Iron(III) Sulfate–Paramagnetic Phase[a]

T, K	δ	ΔE_Q	$\Gamma_{1/2}$	area	χ^2
28.8	0.63	0.32	0.43	7.7	1.2
28.9	0.64	0.33	0.38	8.3	1.1
29.2	0.62	0.32	0.33	7.9	1.1
30.0	0.61	0.31	0.30	7.5	1.1
78	0.60	0.32	0.29	7.6	2.0
300	0.49	0.29	0.29	6.4	0.8

[a] All data in mm/s relative to natural α-iron foil. Area has units of counts·mm/s.

A quantitative measure of the degree of covalency present about an octahedrally coordinated d^5 ion can be calculated from eq 1 which is derived from a molecular orbital description

$$S/S_0 = 1 - 1.2(A_\sigma^2 + 2A_\pi^2 + A_s^2) \qquad (1)$$

of the bonding.[23] In this expression, S is the measured spin, S_0 is the free-ion spin corrected for zero-point spin deviation, and the A_i values are the σ, π, and s covalency parameters. The magnitude of the zero-point spin correction depends upon the structure type, and no suitable calculation is available for anhydrous iron(III) sulfate. In the following discussion an estimated correction of 2.5% has been applied; this has been taken from results on simpler structures.[24]

The covalency parameter sum is calculated as $A_\sigma^2 + 2A_\pi^2 + A_s^2 = 6.1 \pm 1.4\%$. This can be compared with the value of 15.3% found in $Sr_2Fe_2O_5$[24] and values of 10.0 and 11.0% in $LaFeO_3$ and $YFeO_3$, respectively.[25] These three compounds contain FeO_6 octahedra with Fe–O bond lengths similar to those in anhydrous iron(III) sulfate. In the mixed-metal oxides, the negative charge on the oxygen atoms will be greater than that on the sulfate oxygen in iron(III) sulfate. The sulfate group should therefore be less easily polarized leading to a more ionic Fe–O bond, as observed in the lower covalency parameter sum.

Values of covalency parameters determined by this method should be treated with caution. The value obtained depends upon the small difference between the observed moment and the "ideal" moment. It is obviously necessary to measure the moment with great accuracy because small changes in its magnitude lead to large changes in the covalency parameter. The observed moment is very sensitive to the magnetic form factor used, and we believe that uncertainties in the shape of the curve, particularly at high $(\sin\theta)/\lambda$, are a likely source of error in our calculations. A further source of error is the reliability with which the correction for zero-point spin deviation is known. Finally, we have noted that there is a substantial correlation between the temperature factor and the magnetic moment. The temperature factor in turn depends upon the estimated background level under the high-angle Bragg peaks.[26] We estimate that these errors lead to an uncertainty of ±3% in the value of the magnetic moment.

Mössbauer Effect Results. The Mössbauer effect spectra of anhydrous iron(III) sulfate obtained at several temperatures between 300 and 28.8 K are shown in Figure 3. The Mössbauer effect parameters derived from the computed fits to the spectra are given in Table III and the fitted curves are represented by the solid lines shown in Figure 3. The results indicate that anhydrous iron(III) sulfate is paramagnetic at temperatures of 28.8 K and above. The parameters given in Table III assume a fit to two lines with a small quadrupole interaction. An essentially identical set of results at room temperature have been reported by Haven and Noftle.[8] Because monoclinic anhydrous iron(III) sulfate contains two crystallographically different iron(III) sites, we propose that the spectra shown in Figure 3 are composed of two unresolved sets of quadrupole split lines (for a total of four lines) one set of which is associated with each crystallographic iron site. An

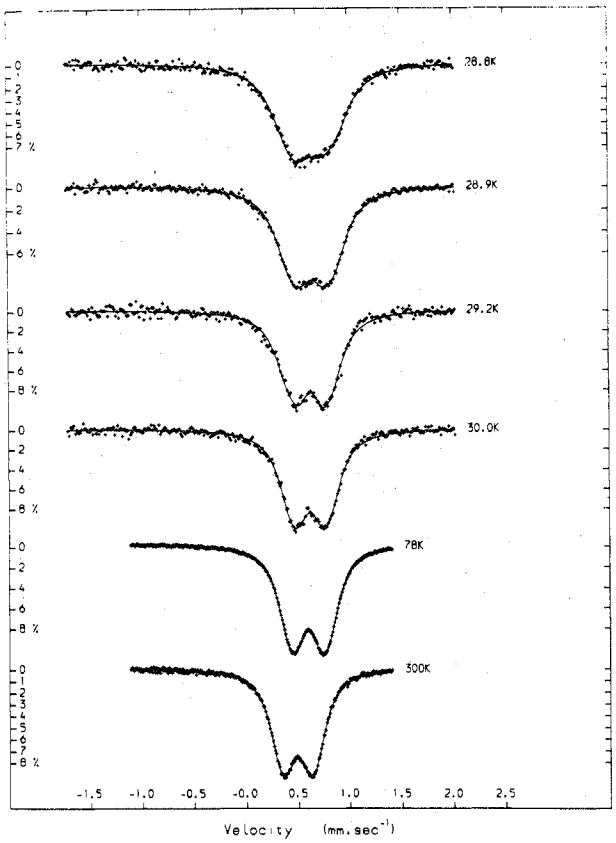

Figure 3. The Mössbauer effect spectra of paramagnetic monoclinic anhydrous iron(III) sulfate obtained at temperatures above 28.8 K.

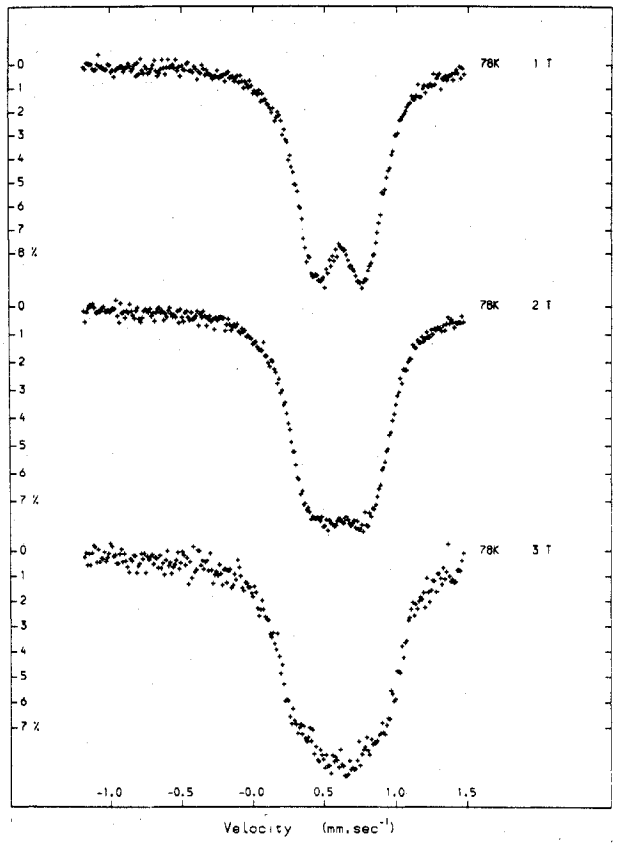

Figure 4. The Mössbauer effect spectra of monoclinic anhydrous iron(III) sulfate at 78 K and in several transverse applied magnetic fields.

alternate interpretation would assign each of the observed lines to one of the crystallographic iron sites with essentially no quadrupole splitting. This assignment would yield quite different isomer shifts for the two sites—a result inconsistent with the very similar average Fe–O bond distances (see Table II) and with low-temperature data presented below. The same conclusion has been reached by Haven and Noftle[8] but is in disagreement with the assignments of A. Bristoti et al.[27] However we believe that the results of the latter authors are probably better evaluated in terms of two sets of quadrupole split lines.

The results presented in Table III are typical of paramagnetic high-spin iron(III) in an essentially octahedral crystal field. The room-temperature isomer shift of 0.49 mm/s is in very good agreement with the observed room-temperature value[28] of 0.45 mm/s for the cubic M(1) site in voltaite, a mineral which contains isolated octahedral FeO_6 units with an average bond distance of 2.004 Å, essentially the same distance as in anhydrous iron(III) sulfate (see Table II). The temperature dependence observed in the isomer shift probably results from a second-order doppler shift. As expected for a $^6A_{1g}$ electronic ground state, the quadrupole interaction does not change with temperature. The increase in area with decreasing temperature indicates that the recoil-free fraction is increasing slowly with decreasing temperature. The rather large line width at 28.8 and 28.9 K is probably a result of the impending magnetic ordering which occurs at ca. 28.7 K.

In an attempt to determine the sign of the quadrupole interaction, we have measured the spectrum of monoclinic anhydrous iron(III) sulfate in several applied fields. The results are presented in Figure 4. Unfortunately the results are not sufficiently resolved to allow the determination of the sign of the quadrupole interaction.

The Mössbauer effect spectra of monoclinic anhydrous iron(III) sulfate at several temperatures from 28.6 to 4.2 K are shown in Figure 5. The results indicate that at these temperatures the material is magnetically ordered. In addition it is immediately apparent, especially at temperatures between 25 and 16 K, that the material exhibits more than the typical six-line magnetic spectrum which would result from the presence of a single uniform internal hyperfine field. In fact the spectra are best understood in terms of two sets of six-line spectra resulting from slightly different internal hyperfine fields, quadrupole shifts, and isomer shifts associated with the two crystallographically different iron sites. There are four possible combinations of internal hyperfine field and quadrupole interaction which are plausible for the observed spectra. We have fitted all of the spectra shown in Figure 5 to each of these four possible combinations and find that only one of these models gives an acceptable fit for all of the spectra. The results of this model are presented in Table IV and are illustrated by the solid lines shown in Figure 5. A Lorentzian distribution of internal hyperfine fields is assumed and accounted for as an incremental line width, $\Delta\Gamma$, in Table IV. The fits obtained were constrained such that only two magnetic spectra were present. No other constraints were applied. In all instances the other models (with different internal hyperfine fields, quadrupole shifts, or isomer shifts) gave significantly higher χ^2 values and results which were inconsistent as a function of temperature. In each spectrum we were forced to conclude that a small amount of a paramagnetic impurity was present. This impurity is most apparent in the 16.1-K spectrum as a weak doublet centered at ca. 0.5 mm/s with a quadrupole splitting of ca. 0.2 mm/s. This impurity, which never consisted of more than 4% of the total absorption area, surprisingly, remains paramagnetic even at 1.2 K. Its identity remains unresolved.

Several aspects of Table IV require discussion. Inspection of this table reveals that there are small differences in the

Table IV. Mössbauer Effect Parameters for Monoclinic Anhydrous Iron(III) Sulfate–Antiferromagnetic Phase[a]

	Fe(1) sublattice							Fe(2) sublattice							absolute	
T, K	δ	H^b	QS	$\Gamma_{1/2}$	$\Delta\Gamma^c$	area	I^d	δ	H^b	QS	$\Gamma_{1/2}$	$\Delta\Gamma^c$	area	I^d	area[e]	χ^2
4.2	0.55	550	−0.04	0.25	0.01	49	1.92	0.61	556	0.03	0.23	0.04	46	0.78	10.0	1.3
10.0	0.56	532	−0.04	0.26	0.01	47	1.39	0.57	543	0.04	0.25	0.02	48	1.33	9.1	1.3
16.1	0.56	473	−0.04	0.25	0.01	42	1.33	0.56	495	0.05	0.27	0.01	52	1.49	8.4	1.6
21.1	0.58	406	−0.05	0.23	0.02	48	1.51	0.57	433	0.05	0.23	0.02	47	1.53	8.4	1.2
24.2	0.58	346	−0.04	0.25	0.02	48	1.50	0.58	373	0.04	0.21	0.06	47	1.40	8.3	1.5
25.8	0.66	290	−0.04	0.22	0.05	47	1.45	0.65	314	0.04	0.24	0.02	48	1.61	8.4	1.3
27.9	0.59	207	−0.04	0.23	0.04	51	1.59	0.60	226	0.04	0.22	0.05	43	1.46	8.1	1.2
28.6	0.59	118	−0.05	0.35	0.03	50	1.84	0.61	130	0.04	0.38	0.05	44	1.47	9.4	1.0

[a] Data in mm/s relative to natural α-iron foil. [b] Internal magnetic hyperfine field in kOe. [c] The incremental line width increase for the outermost magnetic lines. [d] Intensity ratio of line 2 (or 5) to line 3 (or 4). [e] Absolute area in counts·mm/s.

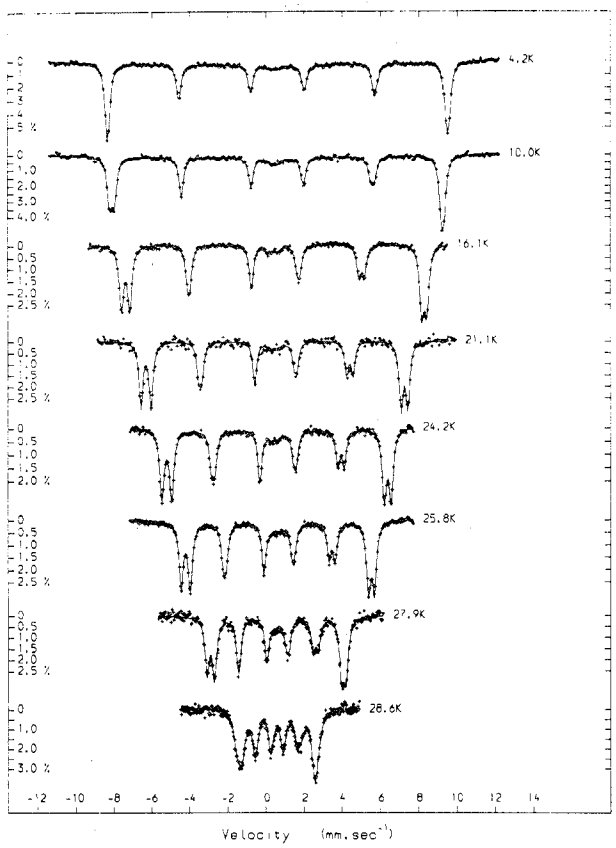

Figure 5. The Mössbauer effect spectra of magnetically ordered monoclinic anhydrous iron(III) sulfate obtained at several temperatures below 28.6 K.

magnetization as a function of temperature for the two different sublattices present in this basically antiferromagnetic material. The two crystallographically different iron sites have essentially the same average Fe–O bond distance. Both the neutron data presented in Table II and the single-crystal X-ray data[10] show that the average Fe(1)–O distance is longer than the average Fe(2)–O distance by only 0.015 Å. In view of this small difference it is not surprising that the isomer shift for each site is essentially identical. Hence, it may not be used to assign the respective lattice sites. The magnitude of the quadrupole shift is also essentially the same at each site. Because it depends upon the angle between the internal hyperfine field and the EFG tensor principal axis, the magnitude of this principal axis, and the magnitude of the asymmetry parameter, the quadrupole shift can not be used to assign the specific internal field to a specific sublattice. Because neither the isomer shift nor the quadrupole interaction may be used in this assignment, we are forced to make the assignment on the basis of a model for the exchange coupling. This model is discussed in detail in a later section and is the basis of the assignments given in Table IV.

We have carried out a calculation of the EFG tensor at the different crystallographic sites in anhydrous iron(III) sulfate. The lattice sum, involving equal charges on the six nearest oxygen atoms, yields $V_{xx} = -0.0057$, $V_{yy} = -0.0420$, and $V_{zz} = 0.0477$ for Fe(1) and $V_{xx} = -0.0012$, $V_{yy} = -0.0263$, and $V_{zz} = 0.0275$ for Fe(2). The matrix representing the principal axes at each site is given in ref 29. Because V_{xx} is very nearly zero, η, the asymmetry parameter, is ca. 1 at each site. This conclusion, which appears to disagree with that of Haven and Noftle,[8] may indicate that it is necessary to include more distant atoms in the lattice sum. The value of η, when used in conjuction with the orientation of the internal hyperfine field determined from the neutron data, and the quadrupole interaction obtained at 28.8 K, permits the calculation[30] of the angle between the internal hyperfine field and the principal axis of the EFG and hence the quadrupole shift. We obtain $\theta = 32°$ and $\phi = 55°$ for Fe(1) and $\theta = 81°$ and $\phi = 7°$ for Fe(2). The resulting quadrupole shifts are +0.07 mm/s for Fe(1) and −0.001 mm/s for Fe(2). These results are in only fair agreement with the observed values of ca. ±0.04 mm/s and again may indicate the need to include more atoms in our lattice sum. Alternately, it may indicate a change in the quadrupole interaction between 28.8 and 4.2 K.

In Table IV the relative intensity of the second (and fifth) line in the magnetic hyperfine spectrum is given as the ratio of this line to the third (and fourth) line in the spectrum. If the internal hyperfine field is normal to the incident Mössbauer γ-ray, this ratio is 4; if it is parallel with the γ-ray, it is zero. In the case of a random polycrystalline sample, the average over all solid angles yields a value of 2 for this ratio.[31] Inspection of Table IV reveals that this ratio is not that expected of a random polycrystalline sample. Again by use of the most accurate data (from 27.9 to 10.0 K), the average ratio for the intensity of line two (and five) is 1.47 for each magnetic sublattice. This indicates that the preparation of our polycrystalline absorbers must yield a slightly nonrandom orientation of the polycrystallites such that, on the average, more of the crystals are aligned so that their magnetization is parallel with the γ-ray. Various methods have been tried to prepare random polycrystalline absorbers with no success to date. We are investigating this effect in more detail as a part of a Mössbauer effect study of single crystals of $Fe_2(SO_4)$. It should be noted that these orientation effects were also observed in the powder neutron-diffraction studies.

Perhaps the most interesting aspect of the magnetic properties of the ordered phase is the nonequivalent internal hyperfine fields found on the two sublattices. A plot of this field as a function of temperature is given for the two sublattices in the lower part of Figure 6. The difference between these two fields is given in the upper part of Figure 6. It is apparent that at the lowest temperatures, the field is close to saturation at a value very near the predicted value of 550 kOe.[32] The plot of the approach of the field to zero at ca. 28.7

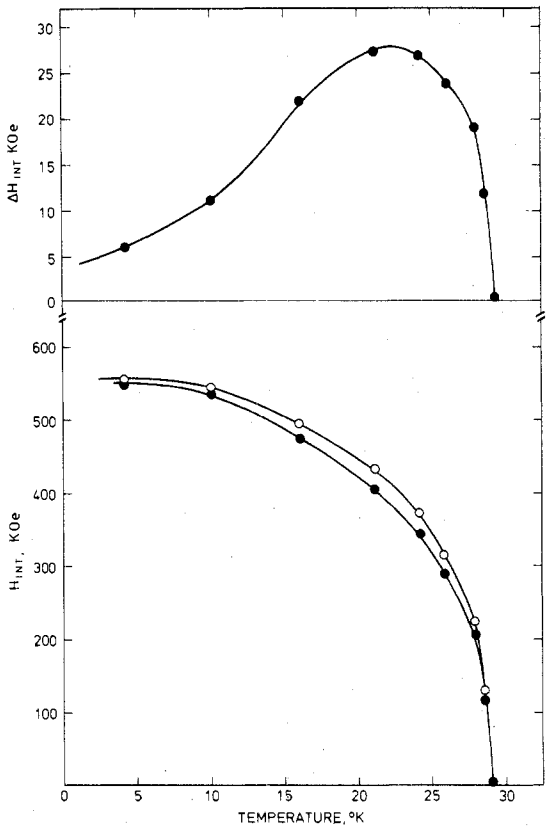

Figure 6. A plot of the internal hyperfine field on each sublattice and the difference between these fields, ΔH_{int}, as a function of temperature.

K is essentially normal to the temperature axis indicating a very sharp Néel point and transition into the ordered phase. As is observed in Figure 6, the maximum difference in the field of the two different sublattices occurs at ca. 23 K with a difference of 27 kOe. This maximum is confirmed by magnetic susceptibility studies described below. It is rather unusual to find that the two sublattices in this antiferromagnet have different internal hyperfine fields at a given temperature. However, it should be noted that the two sublattices in monoclinic, anhydrous iron(III) sulfate have crystallographically different kinds of iron and different exchange pathways between them. Below we propose a model which accounts for the difference in the internal hyperfine field on the two sublattices.

On the basis of the line-profile analysis described above, we have concluded that monoclinic, anhydrous iron(III) sulfate is antiferromagnetically coupled at 4.2 K. This conclusion may be confirmed by measuring the Mössbauer spectrum of this material in an applied field. If the material is ferromagnetic, one would expect the rotation of the internal field directions to reduce the internal hyperfine field. The field is reduced because the Fermi contact term will be opposite in sign to the applied field.[32] In the case of a two-sublattice antiferromagnet, the applied field will add to one sublattice magnetization and substract from the second. In this case, the resulting Mössbauer effect spectrum will exhibit a broadening of the magnetic hyperfine lines, but no decrease in the magnetic splitting is observed—as would be expected for a ferromagnet. Although the powder average obtained for a polycrystalline absorber will decrease the effect of the applied field, the final result will be the same. We have measured the spectrum of anhydrous iron(III) sulfate in an applied field of 1, 3, and 6 T. The results are presented in Table V and the resulting spectra are illustrated in Figure 7.

Because the internal fields are so similar for the two

Table V. Mössbauer Effect Parameters for Monoclinic Iron(III) Sulfate in an Applied Field at 4.2 K[a]

H_{app}	δ	H^b	$\Gamma_{1/2}$	I^c	absolute area[d]	χ^2
0	0.62	560 (3)	0.48	1.40	9.7	1.7
1	0.62	560 (3)	0.48	1.39	9.4	3.2
3	0.62	560 (3)	0.48	0.93	9.7	3.6
6[e]	0.62	564 (3)	0.41	0.81	7.5	1.9

[a] All data in mm/s relative to natural α-iron foil. [b] Internal hyperfine field in kOe. [c] Intensity ratio of line 2 (or 5) to line 3 (or 4). [d] Absolute area in counts·mm/s. [e] Obtained with a separate sample.

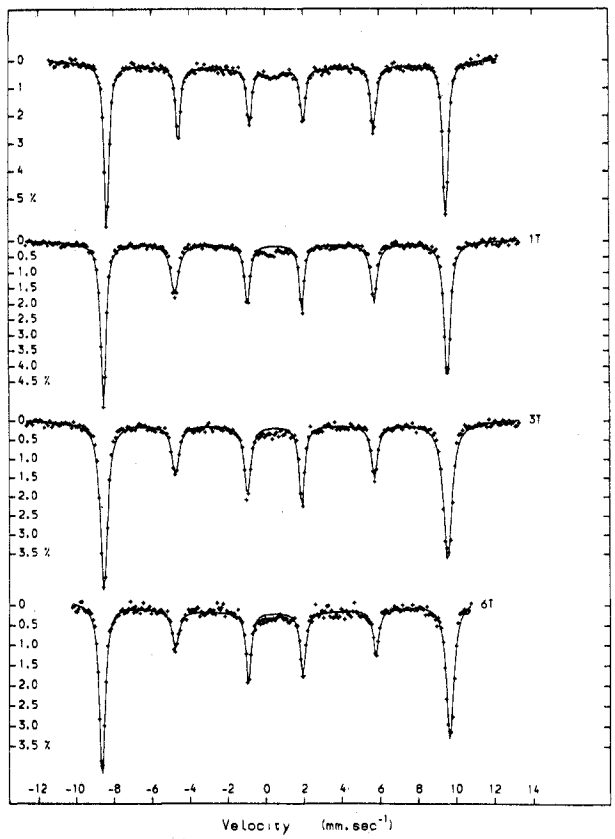

Figure 7. The Mössbauer effect spectra of ordered anhydrous iron(III) sulfate at 4.2 K obtained in a transverse applied magnetic field.

sublattices of anhydrous iron(III) sulfate at 4.2 K, we have modeled the applied-field results to a single magnetic spectrum. As a result, the χ^2 values given in Table V are higher than for the zero-field spectra (Table IV). In addition, this model yields the average of the quadrupole shifts for the two sublattices. All of the fits in Figure 7 indicate a zero quadrupole shift. As expected for an antiferromagnet, the value of the internal hyperfine field remains essentially constant in the presence of the applied field. The values listed in Table V are ca. 1% larger than those found in Table IV because a different sample and fitting model has been used to obtain these values. The relative intensity of the two (and five) line decreases with increasing applied field. If the hyperfine field arrangement in the polycrystalline sample is divided into components parallel and transverse to the applied field, then the behavior of the components can be considered separately. The transverse components will be canted slightly in the direction of the applied field which will increase the relative intensity of lines two and five. However, for the parallel components, if the applied field is sufficient to produce the spin-flop transition, the transverse component of the internal hyperfine field will increase. Although these components will then be canted

Table VI. Magnetic Data for Monoclinic Anhydrous Iron(III) Sulfate

T, K	$\chi_{Fe}' \times 10^6$, cgsu	$1/\chi_{Fe}'$, $cgsu^{-1}$	μ_{eff},[a] μ_B
298.2	11 355	88.07	5.88
279.4	11 815	84.64	5.84
262.6	12 435	80.42	5.85
244.2	13 080	76.45	5.84
224.1	13 985	71.51	5.85
205.4	14 685	68.10	5.81
186.3	16 245	61.56	5.90
167.8	17 250	57.97	5.87
147.8	18 755	53.32	5.87
127.4	20 530	48.71	5.86
103.3	23 420	42.70	5.89
80.4	23 935	38.56	5.80
69.3	28 245	35.40	5.85
55.3	31 885	31.36	5.92
38.4	37 650	26.56	6.02
32.9	44 455	22.50	6.39
30.8	69 250	14.44	7.90
29.1	112 300	8.90	9.99
23.4	116 700	8.57	9.92
21.6	116 200	8.61	9.81
13.1	86 500	11.56	8.11
9.2	61 550	16.25	6.70
6.0	49 740	20.10	5.92
4.3	42 635	23.46	5.42

[a] Calculated from the equation $\mu_{eff} = 2.828[\chi_{Fe}'(T - \Theta)]^{1/2}$ where Θ is −82.0 K.

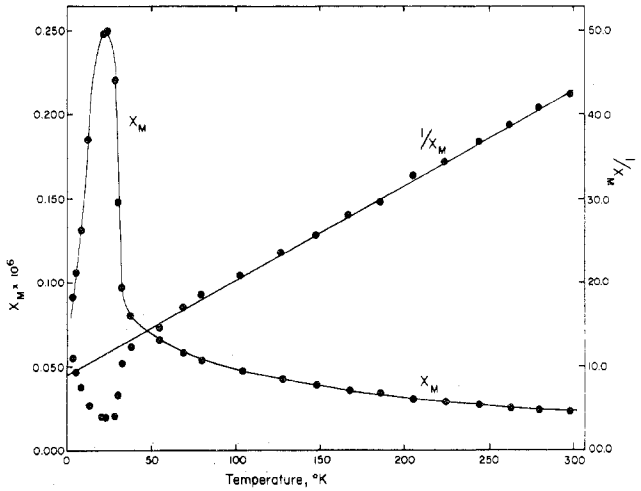

Figure 8. A plot of the molar magnetic susceptibility, χ_M', and the inverse susceptibility of anhydrous iron(III) sulfate as a function of temperature. The linear least-squares line through the inverse susceptibility data is based on the data obtained above 60 K and gives a Θ value of −82.0 K.

slightly in the applied field direction (as mentioned above), the result, considering both components, will be a reduction in the net parallel component which leads to a reduction in the intensity of lines two and five. Apparently, a field of 3 T is sufficient to induce the spin-flop transition in this material.

Magnetic Susceptibility Results. The molar magnetic susceptibility of monoclinic, anhydrous iron(III) sulfate is presented in Table VI and shown in Figure 8. This susceptibility is the field-weighted average of eight applied-field measurements obtained between 1000 and 8000 G. At most temperatures the magnetization increased linearly with the applied field. This is illustrated in Figure 9 for most of the temperatures studied. Rather than discuss these results in terms of molar susceptibility, we have calculated the susceptibility and magnetic moment per iron atom (see Table VI). A plot of $1/\chi_M'$ (see Figure 8) or $1/\chi_{Fe}'$ as a function of

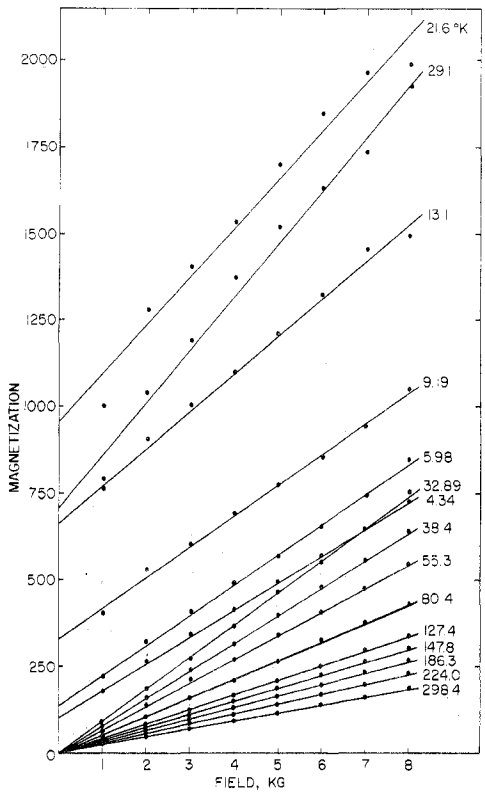

Figure 9. The magnetization of anhydrous iron(III) sulfate as a function of applied field.

temperature yields a large negative Weiss temperature. For reasons described below, we have only used data above 60 K to determine the Curie–Weiss temperature through a linear least-squares extrapolation to zero. The value obtained is −82.0 K and is reasonable for an antiferromagnetic material. If the temperature is corrected for the Weiss field (Table VI), the magnetic moment is ca. 5.9 μ_B and essentially independent of temperature above ca. 40 K. This is, of course, just the effective magnetic moment expected of a high-spin iron(III) compound.

Below ca. 30 K the magnetic susceptibility and moment rise sharply to a maximum at 23.4 K and then decrease just as sharply. This sharp rise at ca. 30 K is not the behavior expected of a typical antiferromagnetic compound but arises because the magnetization is not equivalent in magnitude on the two sublattices of iron(III) sulfate. Below ca. 33 K the Weiss-corrected effective magnetic moment begins to increase above 5.92 μ_B. This is about 5 K above the ordering temperature obtained in the Mössbauer effect studies (see Figure 6). Apparently short-range critical fluctuations are important in this temperature interval.[2] It of course follows that the maximum in the observed susceptibility at 23 K should correspond to the temperature of the maximum difference in magnetization of the two sublattices as is seen in Figure 6. Below 23 K, as the field on the two sublattices begins to saturate toward a value of ca. 550 kOe, the difference decreases and correspondingly the observed susceptibility decreases. This description of the magnetic properties is also confirmed by the magnetization results illustrated in Figure 9. Above the magnetic-ordering temperature there is no spontaneous magnetization, and the induced magnetization extrapolates exactly to zero at a zero applied field. However, below the ordering temperature, the spontaneous magnetization generated on the two antiferromagnetic sublattices is not equivalent, and a net magnetization results at zero applied field. This is of course observed in the extrapolation of the induced magnetization to positive values at zero field (see

Table VII. Magnetic Superexchange Pathways in Anhydrous Iron(III) Sulfate

atom pair	no. of different Fe′ atoms	multiplicity	total no. of exchange paths	exchange type	ave exchange pathway, Å	ave angle at sulfur, deg
Fe(1)-Fe′(1)	3	2	6	ferromagnetic	6.94	110.7
Fe(2)-Fe′(2)	3	2	6	ferromagnetic	6.90	109.9
Fe(1)-Fe′(2)	1	4	4	antiferromagnetic	6.92	109.7
	2	2	4	antiferromagnetic	6.93	108.4
	4	1	4	antiferromagnetic	6.92	109.7

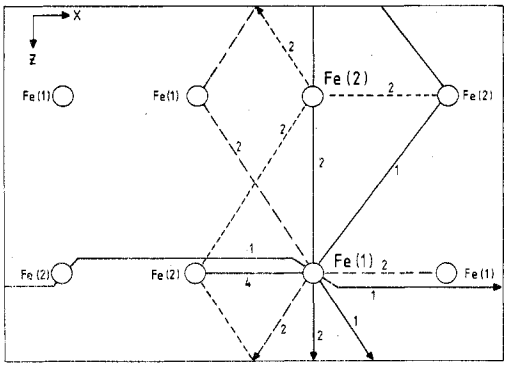

Figure 10. A projection of the iron atomic coordinates with the various superexchange pathways indicated by --- for Fe(1)–Fe(1) linkages, — for Fe(1)–Fe(2) linkages, and - - - for Fe(2)–Fe(2) linkages. The numbers indicate the number of Fe–O–S–O–Fe bridges per path.

Figure 9) for data at 29.1 K and below.

The magnetic susceptibility data indicate an ordering temperature between 30.8 and 29.1 K while the Mössbauer effect data give a value between 28.8 and 28.6 K. The exact reason for this difference is not understood at this time but may be related to the different thermometry methods used in the two studies.

Magnetic Ordering Model. The rather unusual low-temperature magnetic properties of monoclinic, anhydrous iron(III) sulfate call for special discussion. Specifically, we need to understand why the magnetization on the two magnetic sublattices shown in Figure 2 is different between the ordering temperature and 4.2 K. In monoclinic, anhydrous iron(III) sulfate each iron atom is coordinated to six oxygen atoms which are a part of six different sulfate groups (see Figure 2). As a result, each iron atom is connected to ten surrounding iron atoms by 18 "bridging" Fe–O–S–O–Fe linkages. The nature of these connections is described in Table VII and illustrated in Figure 10. This figure is a representation of the unit cell of iron(III) sulfate (see Figure 2) in which we have indicated the superexchange pathways with lines. The number of the bridges between a specific iron atom and a given neighbor varies from 1 to 4. The number of these bridges is indicated in Figure 10. Specifically the Fe(1) site given in bold letters in Figure 10 is connected to three other Fe(1) atoms via two linkages each, for a total of six.[33] These links are shown by the dashed line. In addition the Fe(1) atom is also connected to seven different Fe(2) atoms as shown by the solid lines in Figure 10. This gives a total of 12 different Fe(1)–O–S–O–Fe(2) bridges. It is most interesting that this Fe(1) is connected to one of the Fe(2) sites by four Fe–O–S–O–Fe bridges. Hence the two iron atoms in the lower central portion of Figures 2 and 10 are connected by four bridges while at most two bridges connect the Fe(1) atom to any other iron.

The neutron diffraction results show that the two crystallographically different iron atoms are antiferromagnetically aligned. Because the superexchange pathways between Fe(1) and Fe(1), Fe(1) and Fe(2), and Fe(2) and Fe(2) are rather similar (see Table VII), it is not immediately apparent how the observed antiferromagnetism arises. There are only small variations in the lengths of the Fe(1)–Fe(2) exchange pathways and no significant variations in the Fe–O–S bond distances and angles. We believe that all the Fe···Fe interactions are intrinsically antiferromagnetic but that the resultant antiferromagnetic coupling between the crystallographically different Fe(1) and Fe(2) (which requires that each separate sublattice to be ferromagnetically coupled) stems from the relative numbers of each type of pathway as is illustrated in Figure 10.

In order to account for the differences in the magnetizations on the two sublattices, we again draw attention to the crystallographic distinction between Fe(1) and Fe(2). Because the sites are clearly distinguishable, there is no reason to expect the fields at the two sites to be the same. Perhaps small differences in the superexchange pathways on the same sublattice may account for the difference in magnetization. In general it is expected that this superexchange will be more effective the shorter the exchange pathway and the closer the angle at the sulfur atom is to the tetrahedral angle.[34,35] As is indicated in Table VII, there are a total of six of these paths connecting a given iron to three of its crystallographically equivalent neighbors. These pathways, which involve ferromagnetic interactions, are, however, slightly different in average length and bridging angle at the sulfate for the two sublattices. Specifically, the ferromagnetic superexchange pathway is 0.04 Å longer for the Fe(1) sublattice. Also the average angle at the bridging sulfate for this sublattice is 110.7°, 0.8° further from the tetrahedral angle than is the respective angle for the Fe(2) sublattice. As a result we tentatively propose that the ferromagnetic exchange is stronger on the Fe(2) sublattice than on the Fe(1) sublattice, and at a given temperature it has the largest magnetization. This is the basis for the assignment given in Table VI.

Acknowledgment. It is a pleasure to acknowledge the assistance of and helpful discussions with Drs. K. Ziebeck, P. Day, and R. Chagnon and Mr. B. Laundy and L. Becker during the course of this work. We thank the AERE University Support Group for experimental assistance, the Science Research Council for the provision of the neutron facilities and a research studentship for P.B., and the National Science Foundation for the financial assistance provided through Grant CHE-75-20417.

Registry No. Iron(III) sulfate, 10028-22-5.

References and Notes

(1) (a) Department of Chemistry, University of Missouri-Rolla. (b) Atomic Energy Research Establishment, Harwell. (c) Chemical Crystallography Laboratory, Oxford University. (d) Inorganic Chemistry Laboratory, Oxford University.
(2) L. J. de Jongh and A. R. Miedema, *Adv. Phys.*, **23**, 1 (1974).
(3) E. Stryjewski and N. Giordano, *Adv. Phys.*, **26**, 487 (1977).
(4) R. L. Carlin and A. J. van Duyneveldt, "Magnetic Properties of Transition Metal Compounds", Springer-Verlag, New York, 1977.
(5) J. W. G. Wignall, *J. Chem. Phys.*, **44**, 2462 (1966).
(6) P. Theodorides, *J. Phys. Radium*, **3**, 1 (1922).
(7) S. DeBenedetti, G. Lang, and R. Ingalls, *Phys. Rev. Lett.*, **6**, 60 (1961).
(8) Y. Haven and R. E. Noftle, *J. Chem. Phys.*, **67**, 2825 (1977).
(9) A. R. Champion, R. W. Vaughan, and H. G. Drickamer, *J. Chem. Phys.*, **47**, 2583 (1967).
(10) P. B. Moore and T. Araki, *Neues Jahrb. Mineral. Abh.*, **121**, 208 (1974).
(11) P. C. Christidis and P. J. Rentzeperis, *Z. Kristallogr., Kristallgeom. Kristallphys. Kristallchem.*, **141**, 233 (1975).

(12) A. I. Vogel, "A Textbook of Quantitative Inorganic Analysis", 3rd ed., Longmans, Green and Co., London, 1961, p 398.
(13) A. W. Hewat, personal communication.
(14) B. N. Figgis and R. S. Nyholm, *J. Chem. Soc.*, 4190 (1958); T. H. Geballe and W. F. Giauque, *J. Am. Chem. Soc.*, **74**, 3513 (1952).
(15) P. A. Kokkoros, *Tschermaks Mineral. Petrogr. Mitt.*, **10**, 45 (1965).
(16) H. M. Rietveld, *J. Appl. Crystallogr.*, **2**, 65 (1969).
(17) G. E. Bacon, *Acta Crystallogr., Sect. A*, **28**, 357 (1972).
(18) R. E. Watson and A. J. Freeman, *Acta Crystallogr.*, **14**, 27 (1961).
(19) M. Bonnet, A. Delapalme, F. Tcheou, and H. Fuess, *Proc. Int. Conf. Magn.*, **4**, 251 (1974).
(20) For a discussion of this effect see A. J. Jacobson, "Chemical Applications of Thermal Neutron Scattering", B. T. M. Wills, Ed., Oxford University Press, London, 1973, p 270.
(21) Numbers in parentheses here and elsewhere in this paper indicate estimated deviations in the least significant digits.
(22) P. Battle and A. K. Cheetham, unpublished results.
(23) J. Hubbard and W. Marshall, *Proc. Phys. Soc., London*, **86**, 561 (1965).
(24) C. Greaves, A. J. Jacobson, B. C. Tofield, and B. E. F. Fender, *Acta Crystallogr., Sect. B*, **31**, 641 (1975).
(25) B. C. Tofield and B. E. F. Fender, *J. Phys. Chem. Solids*, **31**, 2741 (1970).
(26) A. K. Cheetham and J. C. Taylor, *J. Solid State Chem.*, **21**, 253 (1977).
(27) A. Bristoti, P. J. Viccaro, J. I. Kunrath, and D. E. Brandao, *Inorg. Nucl. Chem. Lett.*, **11**, 253 (1975).
(28) G. J. Long, G. Longworth, D. Beveridge, and P. Day, submitted for publication in *Inorg. Chem.*
(29) For Fe(1): 0.4830, 0.7754, −0.4068; −0.0675, −0.4962, 0.8656; 0.8730, 0.3906, 0.2920. For Fe(2): 0.9237, −0.1960, 0.3292; 0.0907, 0.9467, 0.3092; −0.3722, −0.2557, 0.8922.
(30) A. J. F. Boyle and H. E. Hall, *Rep. Prog. Phys.*, **25**, 441 (1962); A. Abragam, *C. R. Hebd. Seances Acad. Sci.*, **250**, 4334 (1960).
(31) N. N. Greenwood and T. C. Gibb, "Mössbauer Spectroscopy", Chapman and Hall, London, 1971, p 63; V. I. Goldanski and E. F. Makarov in "Chemical Applications of Mössbauer Spectroscopy", V. I. Goldanski and R. H. Herber, Eds., Academic Press, New York, 1968, p 77.
(32) C. E. Johnson in "Hyperfine Interactions in Excited Nuclei", G. Goldring and R. Kalish, Eds., Gordon and Breach, New York, 1971, p 803.
(33) Those bridges which connect to iron atoms outside the unit cell are translated by one unit cell. These, of course, correspond to links to unique atoms.
(34) P. W. Anderson, "Magnetism", Vol. 1, G. T. Rado and H. Suhl, Eds., Academic Press, 1963, p 25.
(35) J. B. Goodenough, "Magnetism and the Chemical Bond", Wiley, New York, 1963.

Contribution from the Department of Chemistry, University of Ottawa, Ottawa, Ontario, Canada K1N 9B4

Chloro and Oxochloro Anions of Selenium(IV)

PIERRE LAHAIE and JOHN MILNE*

Received August 31, 1978

The Raman spectra of four chloroselenate anions, SeO_2Cl^-, $SeOCl_3^-$, $SeCl_5^-$, and $SeCl_6^{2-}$, two of which have not been reported before (SeO_2Cl^- and $SeCl_5^-$), are discussed. Both solid and MeCN solution spectra with polarization measurements are considered. The spectra are consistent with a pyramidal SeO_2Cl^- ion (C_s), a trigonal-bipyramidal $SeOCl_3^-$ ion with two Cl's axial (C_s), a square-pyramidal $SeCl_5^-$ ion (C_{4v}), and an octahedral $SeCl_6^{2-}$ ion (O_h). Spectral evidence for chloride bridging is found for the compounds $KSeOCl_3$, 8-hydroxyquinolinium oxotrichloroselenate(IV), Et_4NSeCl_5, and $Ph_4AsSeCl_5$.

Introduction

The complex chloro anions of selenium(IV) exhibit a varied and interesting stereochemistry. The stereochemical inactivity of the lone valence electron pair in the hexahalo complexes, SeX_6^{2-} (X = Cl, Br, I), has been a puzzle of longstanding interest.[1,2] Interligand repulsions are sufficiently strong to overcome the stereochemical effect of the lone electron pair in these cases. It would be of interest to determine whether such repulsions are dominant for any of the SeX_5^- series of anions.

The chloro anions derived from $SeOCl_2$ show an intriguing range of stereochemistries. The 1:1 complex of KCl and $SeOCl_2$, which was first prepared by Wise[3] and later formulated as $K[SeOCl_3]$ by Jackson and Smith,[4] has been studied by Raman spectroscopy.[5] The spectrum was assigned assuming monomeric $SeOCl_3^-$ units. However, Cordes[6] has shown that there are essentially infinite chains of $SeOCl_2$ molecules linked by Cl^- bridges in 8-hydroxyquinolinium oxotrichloroselenate(IV). The one known example of an oxotetrachloroselenate(IV) compound, dipyridinium oxotetrachloroselenate(IV), has been shown to consist of cation, chloride, and oxotrichloroselenate(IV) units.[7] Wasif and Salama[8] have shown that only a 1:1 complex is formed between $SeOCl_2$ and Cl^- in Me_2SO.

Complex formation between SeO_2 and X^- (X = Cl, Br, I) in Me_2SO has been studied by UV and visible spectroscopy.[8] Evidence was found only for 1:1 complexes.

Because many of the chloroselenate(IV) anions have not been studied in detail by vibrational spectroscopy and in some cases not at all and since the nature of their stereochemistry is varied and interesting, a program of synthesis and investigation of vibrational spectra of chloro- and oxochloroselenate(IV) anions was begun and is reported here.

Experimental Section

Materials. Selenium dioxide (Alfa) and tetraphenylarsonium (Baker), tetraethylammonium (Baker), and tetramethylammonium (Aldrich) chlorides were all dried overnight on the vacuum line before use. In the case of Et_4NCl, the dehydration was carried out at 0 °C to prevent decomposition. Potassium chloride (BDH, AnalaR) was dried in an oven at 110 °C. Ammonium chloride (BDH, AnalaR) and 8-hydroxyquinoline (Anachemia) were used directly. Hydrogen chloride was from Matheson. Selenium oxychloride (Baker) was vacuum distilled before use. Selenium tetrachloride was prepared according to Novak and Suttle.[9] Anal. Calcd: Cl, 64.24. Found: Cl, 64.20. 8-Hydroxyquinolinium chloride was prepared by crystallizing 8-hydroxyquinoline from an excess of 6 M hydrochloric acid required for neutralization. Anal. Calcd: Cl, 19.52. Found: Cl, 19.01. Acetonitrile was dried by refluxing over P_2O_5 for 1 h and then distilled.

Preparation of Chloroselenate(IV). $MSeO_2Cl$. Tetramethylammonium monochloroselenate(IV) was prepared by dissolving stoichiometric amounts of Me_4NCl and SeO_2 in a minimum amount of MeCN and cooling on ice. White crystals of Me_4NSeO_2Cl were filtered out and dried over P_2O_5 in a vacuum desiccator. Anal. Calcd: Cl, 16.07. Found: Cl, 15.93. The tetraphenylarsonium monochloroselenate(IV) is considerably more soluble in MeCN and was prepared by pumping a stoichiometric mixture in MeCN to dryness.

$MSeOCl_3$. $KSeOCl_3$ was prepared by dissolving KCl in an excess of $SeOCl_2$ by warming. Upon cooling, pale yellow crystals were formed. These were collected by filtration and washed with cold CCl_4. Anal. Calcd: Cl, 44.23. Found: Cl, 43.83. This product could also be prepared from a 1:1 mole ratio of reactants in dry MeCN or as

0020-1669/79/1318-0632$01.00/0